## Research

**Author for correspondence:**
P. Chudzinski
e-mail: pmch.pmch@gmail.com

# Contribution of 1D topological states to the extraordinary thermoelectric properties of Bi$_2$Te$_3$

## P. Chudzinski

School of Mathematics and Physics, Queen's University Belfast, Belfast, UK

PC, 0000-0003-2362-9963

Topological insulators are frequently also one of the best-known thermoelectric materials. It has been recently discovered that in three-dimensional (3D) topological insulators each skew dislocation can host a pair of one-dimensional (1D) topological states—a helical Tomonaga–Luttinger liquid (TLL). We derive exact analytical formulae for thermoelectric Seebeck coefficient in TLL and investigate up to what extent one can ascribe the outstanding thermoelectric properties of Bi$_2$Te$_3$ to these 1D topological states. To this end we take a model of a dense dislocation network and find an analytic formula for an overlap between 1D (the TLL) and 3D electronic states. Our study is applicable to a weakly $n$-doped Bi$_2$Te$_3$ but also to a broader class of nano-structured materials with artificially created 1D systems. Furthermore, our results can be used at finite frequency settings, e.g. to capture transport activated by photo-excitations.

## 1. Introduction

Thermoelectricity, on a fundamental level, gives us a valuable insight into interactions in a system. On the applications side it gives us hope to harvest electric energy from waste heat. The sensitivity to interactions manifest itself in the Mott relation, $S \sim (\partial_\omega \sigma(\omega))/\sigma(\omega)$, which links thermoelectric Seebeck coefficient $S$ and electric conductivity $\sigma$ in the adiabatic regime but also reveals how hard it is to describe (and improve) $S$ from the application viewpoint. In the single-particle picture when $\sigma(\omega) \sim \mathrm{LDOS}(\omega)$, thanks to a singularity in the derivative of its density of states, the one-dimensional (1D) metal could give rise to a huge Seebeck coefficient [1]. This fact has been extensively used in thermoelectricity enhancement by engineering of

low-dimensional nano-structures [2] but the results of these attempts simply proved that unavoidably one needs a full description of electron–electron interactions in these systems. $Bi_2Te_3$, the first discovered strong three-dimensional (3D) topological insulator [3] is also one of the best-known thermoelectric materials at ambient conditions [4]. When it was discovered [5] that in such 3D topological insulator each dislocation will host a pair of counter-propagating 1D topological states, a helical Tomonaga–Luttinger liquid (TLL), there was momentarily an excitement that the outstanding thermoelectric properties of $Bi_2Te_3$ can be finally explained [6]. However, several fundamental obstacles prohibit this simplistic picture. For the case of non-interacting fermions, or in a hydrodynamic liquid with an infinite cut-off, the thermoelectric transport coefficients are zero [7–9], which implies that a meaningful theory that predicts a substantial signal must include interactions and cut-off's in a non-perturbative manner. Furthermore, in order to achieve a non-zero Seebeck coefficient, a mechanism that will induce curvature and backscattering of the 1D states is needed. This is particularly difficult in helical TLL, where backscattering requires a spin flip. Incorporating a uniform spin–orbit coupling in the model, although it modifies the definition of Kramers-invariant variable, is insufficient as it does not allow for backscattering to occur [10].

A series of recent results paved the way to overcome this stalemate. Most importantly it has been recently shown that a new type of Rashba-like spin–orbit coupling is present on a dislocation [11]. The coupling has been shown to be momentum $k$-dependent, so it can be spatially inhomogeneous. If one now considers a periodic modulation of the Burgers vector (possibly accompanied by a local electric field) then the new Rashba term will be also periodically modulated in space. Such modulation can be induced by lattice distortion corresponding to a transverse optical (TO) phonon mode. This, and inelastic character of phonon processes [12,13], is exactly the kind of term [10] required to cause the desired spin-flip process and overcome the topological protection against backscattering [14]. This shall produce finite resistivities and in effect a finite Seebeck coefficient.

Experimentally, it has been recently shown that each twin boundary in $Bi_2Te_3$ consists of a long chain of lattice dislocation [15–17]. This proves that: (i) dislocations are common in $Bi_2Te_3$ and material may host dense networks of dislocations that may turn the topological effect into a volume effect, (ii) one can in principle control distances between dislocations by changing angle between crystal grains. Developments in experiment/numerics have quantified relationship between dislocation and local strain field [18], while emerging field of dislons [19,20] (quanta of dislocation motion) builds a link between the local strain and phonon–phonon interactions on dislocations [21]. Finally, complex band structure of $Bi_2Te_3$ has been explored by advanced DFT methods (GW) [22] and confirmed by ARPES experiments [23,24]. A consensus has emerged that $Bi_2Te_3$ is an indirect narrow gap semiconductor with a bottom of a conduction band slightly off the Brillouin zone centre [22].

These achievements, in seemingly unrelated areas, have set up the following challenge for many body theory: to compute Seebeck effect in a helical TLL in a strong interaction, strong lattice anharmonicity regime accounting for the fact that the helical TLL states exist only in a finite-energy window (of order $\Lambda_0 \approx 0.25\,\text{eV}$) where they do not decay into energy-momentum matching bulk states. One also needs a good description of a dense network of dislocations to assess the feasibility of our theoretical proposal. In this paper, we give an analytical formula for the strength of Seebeck coefficient due to network of helical 1D states at arbitrary frequency and temperature. The calculation proceeds in two stages: in the first stage, we compute Seebeck coefficient of a single TLL state on a dislocation, while in the second stage we compute tunnelling probability between 3D states (with a given Fermi momentum $k_F^{3D}$) and the states localized on 1D dislocations' array.

## 2. Model

Our system consist of three parts: the 3D dilute electronic liquid from bulk conduction band with free fermion Hamiltonian $H_{3D} = \sum_k E_{\text{DFT}}^{(3D)}(k)c^\dagger(k)c(k)$, the helical TLL $H_{\text{TLL}}^{1D}$ (from the topological

states on dislocation) and the TO phonons described by $H_{ph}$. The 1D theory is written in terms of collective modes, the canonically conjugate bosonic fields $\phi_\nu(x)$ and $\theta_\nu(x)$, with $\Pi_\nu(x) = \partial_x \theta_\nu(x)$. These fields are directly related to the respective densities $\partial_x \phi_\nu(x) = -\pi \rho_\nu(x)$. Then the TLL Hamiltonian reads:

$$H_{\mathrm{TLL}}^{1D} = \sum_\nu \int \frac{dx}{2\pi} \left[ (v_\nu K_\nu)(\pi \Pi_\nu)^2 + \left( \frac{v_\nu}{K_\nu} \right) (\partial_x \phi_\nu)^2 \right], \tag{2.1}$$

where $v_\nu$, $K_\nu$ are velocity and TLL parameter for each collective $\nu$-mode that constitutes our hydrodynamic liquid. For the helical TLL, because fermion spin and chirality are locked, there is only one mode so we drop the $\nu$ index in the following. Electron–electron interactions that have purely forward character (due to the topological protection) are incorporated in $K = \sqrt{(1-g)/(1+g)}$ where $g = V_{\mathrm{Coul}}(q \to 0)$.

The TO phonon branch, considered here, in $Bi_2Te_3$ has the following properties: (i) local boson density is well-defined quantity as it corresponds to an amplitude of a local atomic oscillation within a unit cell; (ii) these oscillations modify locally Burgers distortion and so the 'new-Rashba' term; (iii) resonant bond character of the crystal lattice vibrations [25] softens $\omega_0(q=0)$; (iv) when a TO phonon is being emitted/absorbed, causing electron backscattering from $+k_F$ to $-k_F$, then the dispersion $\omega(q_0 \approx 2k_F)$ falls in the linear dispersion range (because of a typical available $k_F$ for our specific TLL). Hence the conditions to use the TLL theory for bosons are fulfilled and their Hamiltonian is:

$$H_{ph} = \int \frac{dx}{2\pi} \left[ (v_{ph} K_{ph})(\pi \Pi_{ph})^2 + \left( \frac{v_{ph}}{K_{ph}} \right) (\partial_x \phi_{ph})^2 \right], \tag{2.2}$$

where $\nabla \phi_{ph}$ describes the density of the *local Bi − Te* oscillations in a given, $x_i$th, unit cell and the key advantage of using the TLL formalism is that any anharmonicity (which one expects to be large on the dislocation [19,20]) can be captured by an appropriate choice of the TLL parameter $K_{ph}$. In the following, we take $K_{ph} \approx 1$ which corresponds to hard-core bosons. The electron–phonon coupling reads:

$$H_R = \frac{g_R}{2\pi a} \int dx \partial \phi_{ph}(x) \exp(\iota \phi(x)), \tag{2.3}$$

where we assumed, in accordance with the discussion in the Introduction, that the phenomenon is proportional to the amplitude of distortion ≡ density (spectral weight) of the TO phonons at a given point $n_{ph} = \partial \phi_{ph}(x)$. The amplitude of the process $g_R = V_R/\Lambda$ where $V_R$ has to be found from material specific *ab-initio* calculation, in analogy with those in [11]. We note that $V_R$ is of the same order as spin–orbit coupling in a given material and in $Bi_2Te_3$ while the spin–orbit coupling is also the underlying reason of band gap opening $\Delta_b$. Since $\Delta_b$ determines the $\Lambda$ UV-cut-off of the 1D hydrodynamics, the $g_R$ is expected to be not far from one. The filling of the system is incommensurate so we do not expect equation (2.3) to open 1D many-body gap at $E_F$, for a finite $\omega_0$ (non-adiabatic regime) the coupling is marginal [26].

## 3. Results for a single helical TLL

This situation described in the previous section is ideally suited to employ memory function formalism [27,28] where a single well-defined perturbation breaks the perfect conductivity of TLL. The charge/heat conductivities matrix is then expressed as:

$$\hat{\sigma}(q, \omega; T) = \hat{\chi}(T)(-i\omega \hat{\chi}(T) + \hat{M}(q, \omega))\hat{\chi}(T), \tag{3.1}$$

where $\hat{M}(q, \omega)$ and static susceptibilities $\hat{\chi}(T)$ are $2 \times 2$ matrix as there are two forces ($\nabla E_x$ and $\nabla T$) and two currents (electric and heat). The off-diagonal, thermoelectric conductivities, are equal by Onsager relation. The entries of $\hat{M}(q, \omega)$ are memory functions, i.e. meromorphic functions each equal to a correlator of force-operators $M_{i,l}(q, \omega) = (\langle F_i F_l \rangle|_{q,\omega} - \langle F_i F_l \rangle|_{0,0})$ where the $\langle \rangle$ are computed for $H_{\mathrm{TLL}}$. The force-operator $F_i(x, t) = [j_i(x, t), H_{\mathrm{tot}}(x, t)]$, where $H_{\mathrm{tot}} = H_{\mathrm{TLL}}^{1D} + H_{ph} + H_R$, selects the term in the Hamiltonian that does not commute with the respective

current, $i, l = \sigma, \kappa$. The Seebeck coefficient, defined in a stationary situation where both currents are zero (compensating forces), can be expressed as a ratio of the off-diagonal thermoelectric conductivity term $\sigma_{\sigma\kappa}$ and electric conductivity $\sigma_\sigma$. Usually from the TLL description only the asymptotic behaviour at $T, \omega \to 0$ is extracted. However, for the purpose of this study, to be able to make a valid comparison with experiments, a full functional description valid at intermediate temperatures and frequencies is necessary. Explicit analytic expressions for $F_i(x, t)$ are given in appendix A. We used conformal field theory transformation to obtain the expressions valid at finite temperatures. In order to substitute these to equation (3.1), we need the Fourier transforms. Finding analytic form of the hyperbolic functions' transforms is the key outcome of our study. The $\int \exp(\mathrm{i}(q'x + \omega t)\langle F_i(x, t)F_l(0, 0)\rangle$ can be expressed as a convolution of electronic and phononic parts and for the uniform response $q' \to 0$ is an integral:

$$
\begin{aligned}
M_{\sigma\kappa}(\omega', T) = M^{(0)} T^{2K+2+1-3} \int \mathrm{d}q \, \mathrm{d}w \\
\times \left[ \Pi^{(\mathrm{ph})} \left( \frac{-v_{\mathrm{ph}}q + (w - \omega')}{T}, K_{\mathrm{ph}} \right) \Pi^{(\mathrm{ph})} \left( \frac{v_{\mathrm{ph}}q + (w - \omega')}{T}, K_{\mathrm{ph}} \right) \right. \\
\times \left( \Gamma^{(\mathrm{el})} \left( \frac{w - qV_F}{T}, K + 1 \right) \Pi^{(\mathrm{el})} \left( \frac{qV_F + w}{T}, K \right) \right. \\
\left. \left. + \Gamma^{(\mathrm{el})} \left( \frac{qV_F + w}{T}, K + 1 \right) \Pi^{(\mathrm{el})} \left( \frac{w - qV_F}{T}, K \right) \right) \right]
\end{aligned}
\tag{3.2}
$$

and

$$
\begin{aligned}
M_{\kappa\kappa}(\omega', T) = M^{(0\kappa)} T^{2K+2+2-3} \int \mathrm{d}q \, \mathrm{d}w \\
\times \left[ \Pi^{(\mathrm{ph})} \left( \frac{-v_{\mathrm{ph}}q + (w - \omega')}{T}, K_{\mathrm{ph}} \right) \Pi^{(\mathrm{ph})} \left( \frac{v_{\mathrm{ph}}q + (w - \omega')}{T}, K_{\mathrm{ph}} \right) \right. \\
\times \left( \Gamma^{(\mathrm{el})} \left( \frac{qV_F + w}{T}, K + 1 \right) \Gamma^{(\mathrm{el})} \left( \frac{w - qV_F}{T}, K + 1 \right) \right. \\
+ \Gamma_Q^{(\mathrm{el})} \left( \frac{w - qV_F}{T}, K \right) \Pi^{(\mathrm{el})} \left( \frac{qV_F + w}{T}, K \right) \\
+ \Gamma_Q^{(\mathrm{el})} \left( \frac{qV_F + w}{T}, K \right) \Pi^{(\mathrm{el})} \left( \frac{w - qV_F}{T}, K \right) \\
+ \Pi^{(\mathrm{el})} \left( \frac{qV_F + w}{T}, K \right) \Pi^{(\mathrm{el})} \left( \frac{w - qV_F}{T}, K + 2 \right) \\
\left. \left. + \Pi^{(\mathrm{el})} \left( \frac{qV_F + w}{T}, K \right) \Pi^{(\mathrm{el})} \left( \frac{w - qV_F}{T}, K + 2 \right) \right) \right]
\end{aligned}
\tag{3.3}
$$

where the Fourier transforms of hyperbolic functions are $\Pi^{(\mathrm{el})}(z, K_r) = 2^{K_r} \frac{\beta\sqrt{v}}{2\pi} B_{(0, \exp(-\xi_{\mathrm{tr}}^{\mathrm{UV}} T))} \left( \frac{\pi K_r + \mathrm{i}z}{2\pi}, 1 - K_r \right)$, $\Pi^{(\mathrm{ph})}(z, K_r) = 2^1 \frac{\beta\sqrt{v_{\mathrm{ph}}}}{2\pi} B_{(\exp(-\xi_{\mathrm{tr}}^{\mathrm{IR}} T), 1.0)} \left( \frac{\pi K_r + \mathrm{i}z}{2\pi}, 1 - K_r \right)$ and:

$$
\begin{aligned}
\Gamma^{(\mathrm{el})}(z, K_r) = 2^{K_r + 1} \frac{\beta\sqrt{v}}{2\pi} B_{(0, \exp(-\xi_{\mathrm{tr}}^{\mathrm{UV}} T))} \left( \frac{\pi K_r + \mathrm{i}z}{2\pi}, -K_r \right) \\
+ 2^{K_r + 1} \frac{\beta\sqrt{v}}{2\pi} B_{(0, \exp(-\xi_{\mathrm{tr}}^{\mathrm{UV}} T))} \left( \frac{\pi K_r + \mathrm{i}z}{2\pi} + 1, -K_r \right) \\
\Gamma_Q^{(\mathrm{el})}(z, K_r) = 2^{K_r} \frac{\beta\sqrt{v}}{2\pi} \frac{(\mathrm{e}/2)^{-K_r - 2}}{(K_r - \mathrm{i}z)(1 + \mathrm{e}^2)^2}
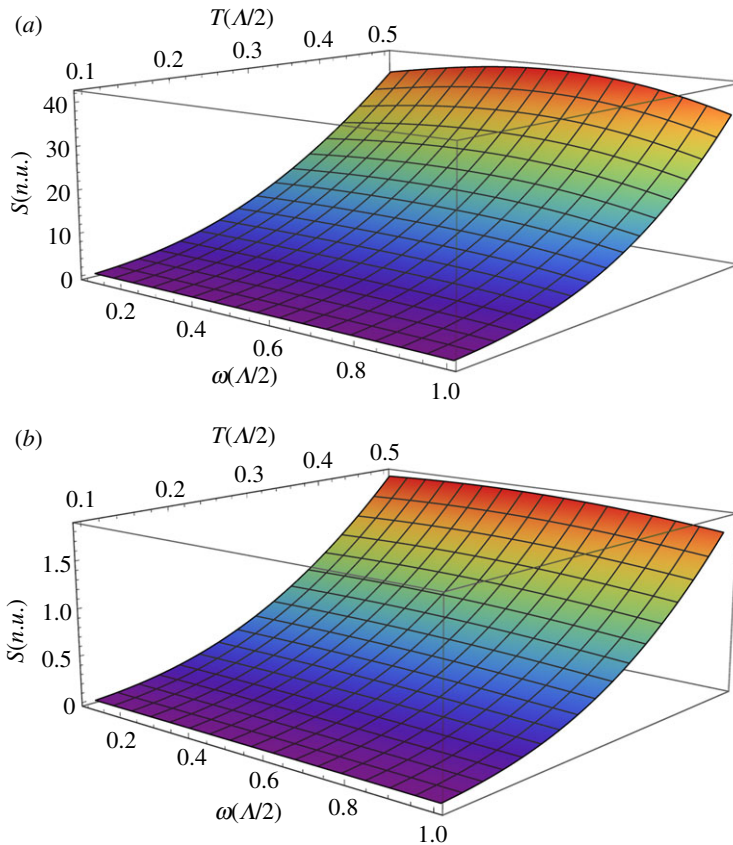\end{aligned}
$$

**Figure 1.** Seebeck coefficients calculated for 1D helical TLL subjected to Rashba-type non-uniform spin−orbit coupling $V_R$. It is given in natural units and should be multiplied by $g_R^2$ where $g_R = V_R/\Lambda$. Here we compare the strength of thermoelectric effect for two different values of TLL parameter $K = 0.3$ (a) and $K = 0.7$ (b). (Online version in colour.)

$$\times F_1 \left( \frac{1}{2}(K_r - \mathrm{i}z); -2, K_r + 2; \frac{1}{2}(K_r - \mathrm{i}z + 2); \right.$$

$$\left. -\frac{1}{\exp(-2(\exp(-\xi_{\mathrm{tr}}^{\mathrm{UV}}T)))}, \frac{1}{\exp(-2(\exp(-\xi_{\mathrm{tr}}^{\mathrm{UV}}T)))} \right) \tag{3.4}$$

where $B_{x_1,x_2}(a,b)$ indicates the generalized incomplete *Beta* function and $F_1(a;b;c;d;x_1,x_2)$ is the Appell hypergeometric function. The temperature independent amplitudes $M^{(0)}$, $M^{(0\kappa)}$ are given in appendix A. This result generalizes well-known single-mode TLL susceptibilities in two ways: (i) it incorporates IR and UV transport cut-off's $-\xi_{\mathrm{tr}}^{\mathrm{UV,IR}}$ which in our problem are very close to the considered temperature/frequency range; (ii) we have here Fourier transforms of the 'vertex' functions[1] $\sim \partial_x G_{\mathrm{TLL}}(x,t)$.

By substituting this into equation (3.1), we obtain a closed analytical formula for the Seebeck coefficient of TLL. We plot the result in figure 1. Since in our calculations we took $\hbar = e = k_B = 1$, then the Seebeck coefficient is given in its natural units $1 n.u. = 28.6 \, (\mu V/K) g_R^2$. Hence, if indeed $g_R \sim O(1)$, then the amplitude of the effect induced by dislocations can be quite substantial $10^3 \, \mu V/K$ which is on a par with the best thermoelectric materials. On both panels, we observe an increasing trend with temperature and a broad maximum as a function of frequency. Remarkably,

[1] We introduce here notion of the 'vertex' by using electron–phonon Ward identities definition, while in a pure electronic system that obeys Dzyaloshinskii–Larkin theorem the standard (non-transport) vertex functions are zero in TLL because RPA is exact and the chiral densities are conserved.

Seebeck effect increases (by an order of magnitude) when the TLL $K$ parameters decreases, i.e. electron–electron interactions are stronger. Since the main factor that decreases $K$ are long-range Coulomb-type interactions then, assuming that the typical length of dislocation is large, it will be screening that determines the TLL parameter. This depends on the density of 3D carriers. We then predict that the Seebeck effect of dislocations will dramatically increase as the chemical potential approaches the conduction band minimum (CBM).

# 4. A network of dislocations

We can now move to the realistic setting where a network of dislocation is present in a weakly $n$-doped $Bi_2Te_3$ (figure 2). Here we assume the following transport mechanism [29]: an external electrode is connected to the 3D bulk states and these electrons, as they propagate through the sample, tunnel into the 1D dislocation states where the large thermoelectric coefficient can be harvested. We now incorporate the tunnelling Hamiltonian into our description $H_{tun} = \sum_i t_{tun}(c^{\dagger(3D)}(r_{\perp i})c^{(1D)}(r_{\perp i}) + h.c.)$. From the standard procedure of constructing a second quantization Hamiltonian, the $t_{tun} \equiv$ probability of tunnelling, is equal to an overlap between 3D and 1D wave functions on a given dislocation $\int dr_\perp \psi^{*3D}(r_\perp - r_{\perp i})\psi_{1D}(r_\perp - r_{\perp i})$. Taking $\psi_{1D}(r_\perp) = 0$ if $r_\perp > R$ and constant inside this cylinder, implies that $t_{tun}$ is proportional to an amplitude of the 3D wave at the dislocation. The 3D electrons are primarily in the conduction band Bloch plane-wave states $\Psi_{1st}^{3D}(r) \sim \sum_{k \in k_{Fi}} \exp(ikr)$, but while the Dirac 1D state is present around the $\Gamma$ point,[2] the CBM is located $\approx \pi/6BZ$ away. The quasi-momentum conservation inhibits direct tunnelling from the primary wave when $k_\perp^{(3D)}(CBM) \neq k_\perp^{(1D)}(\Gamma)$ because the two envelopes do not match. There are however also secondary $\psi_{2nd}^{3D}(r_\perp)$, localized waves present due to multiple electron's wave scattering from the dislocations network.

We take a plane wave coming from a pure crystal and compute multi-site diffraction pattern on cylindrical obstacles. The size of dislocations, distances between them and the Bloch wavelength are all comparable so one cannot consider a point-type wave-scattering but instead needs to use Fresnel diffraction of electronic waves. Such tunnelling problem between 3D wave and 1D localized states has been solved in a closed analytical form in [30]. The solution for the Fresnel diffraction on a circular aperture can be expressed as [31]:

$$\psi_{2nd}(r) = \sum_{k_i}(\sin(N_{\bar{F}}^2(1 + (r/R)^2)/2) + U_1(2N_{\bar{F}}, 2N_{\bar{F}}r/R))$$

$$- i(\cos(N_{\bar{F}}^2(1 + (r/R)^2)/2) - U_2(2N_{\bar{F}}, 2N_{\bar{F}}r/R)) \quad (4.1)$$

here $R$ is the radius of the dislocation, $r$ is a distance within the plane perpendicular to dislocation, $N_{\bar{F}}(k_i) = R^2/(\lambda \Lambda^{-1})$ is the Fresnel number, with $\lambda = \pi/k_i$ a wavelength of a Bloch-electron. To sum over $k_i$ we take two $k_F$'s at two sides of CBM along the direction of line of dislocations (presumably along the twin grain boundary). $U_{1,2}$ are Lommel functions of two arguments, $U_n(w, z) \approx \sum_{m=0}^{\infty}(w/z)^{n+2m}J_{n+2m}(z)$, here $J_{n+2m}(z)$ is a Bessel function of the first kind, they have a damped (weakly aperiodic) oscillatory behaviour. Superposition of waves scattered on all dislocations gives the total amplitude $\Psi_{2nd}(r) = \sum_j \psi_{2nd}(r + jd)$ since each 1D system (with radius $R$) scatters electronic waves and hence becomes a source of an electronic wave $\psi_{2nd}(r)$. Since we are working at the very bottom of the conduction band we need to include Sommerfeld expansion for the temperature dependence of chemical potential.[3] As a result the $k_F$ does depend on temperature and in this indirect way temperature enters also equation (4.1).

---

[2]If we take moderately anharmonic lattice then 1D electronic wave function in $r_\perp$ plane is a combination of Hermite polynomials which can be approximated by a $Box(r_\perp/R_0)$ function and whose Fourier transform is $Sinc(q_\perp)$, negative for $q_\perp \approx \pi/R_0$, so an overlap with any wave-packet at momentum of a fraction of BZ will be suppressed.

[3]In addition, there are DFT results for temperature dependence of the gap [32], that lead to similar effect.
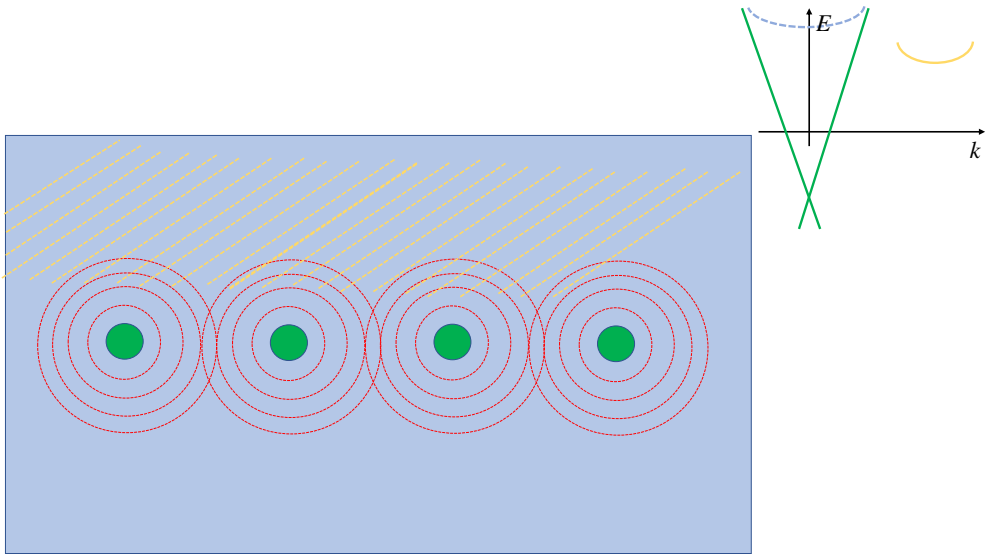
**Figure 2.** Schematic model for the problem of tunnelling of 3D electrons into 1D dislocation states. The plane perpendicular to the dislocation axis is shown. The incoming primary bulk wave $\Psi_{1st}^{3D}$ (yellow dashed lines indicating its nodes) is scattered on a chain of dislocations (green circles for the cross-section of cylinders) that is present on a crystalline twin-boundary. As a result of electronic wave diffraction a secondary wave $\Psi_{2nd}^{3D}$ is produced (red dashed lines). Inset shows a sketch of $Bi_2Te_3$ band structure with 1D states shown in green and bottom of conduction band shown in yellow to match the colour scheme on the main panel. (Online version in colour.)

We can now combine equation (3.1) (with equations (3.2)–(3.4)) and equation (4.1) to find the full temperature dependence of the Seebeck coefficient. The result of this calculation is shown in figure 3. We see that instead of monotonically increasing $S(T)$ (as in figure 1) we have a broad maximum which appears at around $0.25 \Lambda_0/2 \approx 350 \, K$ which is in a reasonable agreement with experiments. Remarkably, we also observe an evidence of the electronic waves interference phenomena—the dependence on a distance between the dislocation is not monotonically increasing, as one would naively expect, but instead there is a complicated dependence with a well pronounced minimum at smaller distances. This is valuable information for the experimentalist: if an experiment is performed such that density of dislocation is varied in a controllable manner then one may find the system in a counter-intuitive regime where increasing the density reduces the Seebeck signal. We show here that this should not disprove the fact that there is a substantial contribution to Seebeck coefficient from dislocation. We also note that for the realistic parameters taken from experiment [15] the amplitude of the effect is massively reduced, it becomes of order of $10 \, \mu V \, K^{-1}$. This is in agreement with the amplitudes that were experimentally reported. The bottleneck of the transport mechanism is not an intrinsic property of Seebeck effect on a dislocation (which is by itself large) but instead it is suppressed by the extrinsic tunnelling amplitude. This can be in principle modified by engineering methods. To explore this, we propose a hypothesis that the drastic suppression of the tunnelling amplitude is related to two electronic waves $k_{CBM} \pm k_F^{(3D)}$ destructively interfering. To validate it we perform another calculation where one of the amplitudes is enlarged with respect to another. This is achievable, in our particular case, since $k_{CBM} - k_F^{(3D)} \approx 1/6BZ$ so adding a superstructure with $\times 6$ periodicity can increase one of the amplitudes. An extra level of complexity that needs to be accounted here is due to an appearance of higher harmonics with momenta $k_n = k_{CBM} - k_F^{(3D)} + n \cdot 1/6BZ$. The result of this calculation is shown on the bottom panel. We see that large values of Seebeck coefficient are recovered. This suggest the realistic way to harvest massive Seebeck coefficient from the dislocations.
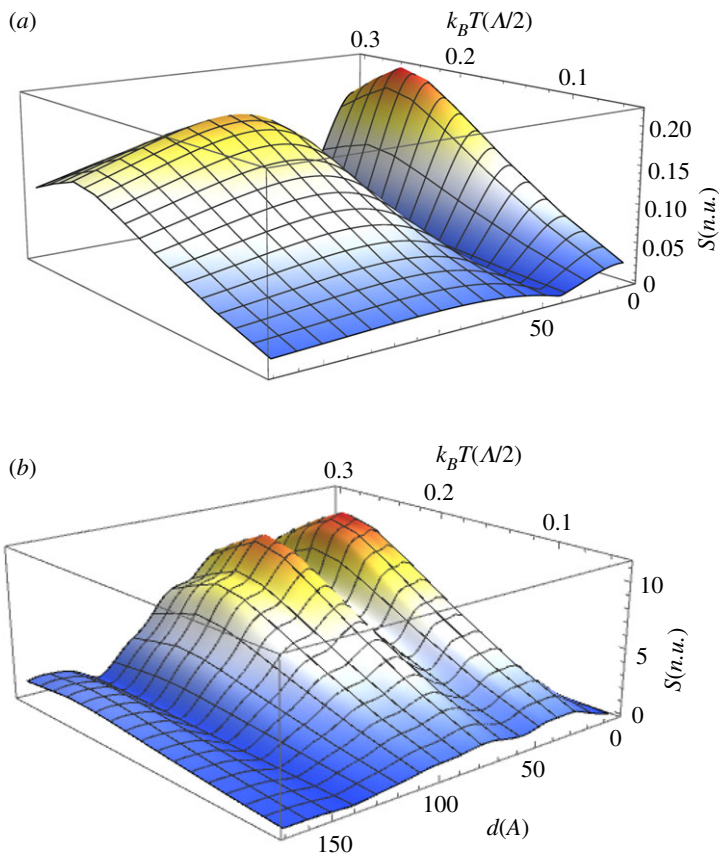
**Figure 3.** Seebeck coefficients, shown as a function of temperature and the inter-dislocation distance, calculated for a network of 1D dislocation embedded in a dilute 3D electron gas. In panel (*a*) we take realistic parameters for $Bi_2Te_3$ while in panel (*b*) we tune the valley position to optimize the tunnelling probability (see text). (Online version in colour.)

## 5. Conclusion

To conclude, firstly we have derived the exact analytic expressions for Fourier transforms of generalized correlation functions, equation (3.4), and for conductivity tensor, equations (3.2) and (3.3), in TLL. The results of these show a dramatic departure from the prediction based on the Mott relation—$\sigma(\omega) \sim \omega^a \implies S(\omega) \sim 1/\omega$, which shows that our formalism is able to capture profoundly non-adiabatic effects. Secondly, we have derived analytic formulas for tunnelling between 3D electron liquid and a network of 1D TLLs. These are necessary ingredient in any transport device based on the 1D nano-structured states. Altogether the analytic solution allowed us to quantify the importance of topological states in thermoelectricity, provide an interpretation of recent experiments [15–17] in $Bi_2Te_3$ and a pathway for future nano-structuring improvements that are available to be harvested.

With analytical formulae derived here we provide a tool that can be used to model various experimental settings. Our study gives a key ingredient, the Seebeck coefficient of the entire array of 1D dislocations, to compute the thermoelectric properties of polycrystalline $Bi_2Te_3$, or more generally any 3D topological insulator. This is the basic unit through which the thermoelectricity is harvested in an extremely weakly doped material. Considering a polycrystal as a huge network of grain boundaries consisting of such basic units opens the way for large-scale physics and engineering simulations that shall give numerical estimates for various polycrystalline realizations. We hope that our study will inspire such future advancements.

## Appendix A. Derivation of the memory function Fourier transforms

The 'force operators' have the following form in the bosonization language:

$$F_\sigma(x,t) = \frac{-ig_R 2KV_F}{2\pi a} \int dx (\partial \phi_{ph}(x) \exp(i\phi(x)) - h.c.) \tag{A 1}$$

and

$$F_\kappa(x,t) = \frac{-ig_R 2V_F^2}{2\pi a} \int dx (\partial \phi_{ph}(x) \partial \phi(x) \exp(i\phi(x)) - h.c.) \tag{A 2}$$

The correlation functions of force operators are computed for $H_{TLL} + H_{ph}$ theory and are known. With the help of CFT, by the mapping a 2D $z = x \pm i\tau$ plane onto a finite size stripe $z \rightarrow \mathrm{Exp}[-2\pi z/\tau_0]$ with $\tau_0 = \beta$, one can compute their finite temperature correlation functions on the $(x,t)$ plane:

$$M_{\sigma\kappa}(x,t) = M^{(0)} T^{2K+2+1} (\mathrm{Sinh}(\xi_{-ph})\mathrm{Sinh}(\xi_{+ph}))^{-K_{ph}}$$
$$\times [\mathrm{Sinh}(\xi_-)^{-K}\mathrm{Cosh}(\xi_+)\mathrm{Sinh}(\xi_+)^{-(K+1)} + (\xi_+ \leftrightarrow \xi_-)] \tag{A 3}$$

and

$$M_{\kappa\kappa}(x,t) = M^{(0\kappa)} T^{2K+2+2} (\mathrm{Sinh}(\xi_{-ph})\mathrm{Sinh}(\xi_{+ph}))^{-K_{ph}}$$
$$\times [K\{\mathrm{Coth}^2(\xi_-)\mathrm{Sinh}(\xi_-)^{-K}\mathrm{Sinh}(\xi_+)^{-K} + (\xi_+ \leftrightarrow \xi_-)\}$$
$$+ K\mathrm{Coth}(\xi_-)\mathrm{Sinh}(\xi_-)^{-K}\mathrm{Coth}(\xi_+)\mathrm{Sinh}(\xi_+)^{-K}$$
$$+ \mathrm{Sinh}(\xi_+)^{-(K+2)}\mathrm{Sinh}(\xi_-)^{-K} + (\xi_+ \leftrightarrow \xi_-)], \tag{A 4}$$

where $M^{(0)}$, $M^{(0\kappa)}$ are temperature-independent amplitudes $M^{(0)} = (g_R^2 2K^2 V_F^3 (\pi a)^{2K+1}(\pi a_{ph})^2)/(2\pi v_{ph} a)^2$ and $M^{(0\kappa)} = (g_R^2 2K V_F^4 (\pi a)^{2K+2}(\pi a_{ph})^2)/(2\pi v_{ph} a)^2$. These expression are equivalent to those in Ref. [28] but re-written in a form more amenable to perform the Fourier transforms. We introduced variables $\xi_{\pm(,ph)} = T(x \pm v_{(,ph)}t)$.

A comment has to be made on the validity of using the TLL correlations for the phonon system. Conventionally, bosonization method is not used for phonons. One problem is to define what the density $\nabla\phi_{ph} \sim \rho_{ph}(x)$ should physically correspond to. A second problem comes from difficulty of reaching the hydrodynamic regime. Phonons are inherently interacting particles because when we define a lattice oscillation in a parabolic potential then the energy of N phonons in the $q$-mode and $N+1$ phonons in the $q$-mode are different, the difference equals $\omega_q$. Then for the phonon exchange process $b_{q+\delta q}^\dagger b_q b_{q'-\delta q}^\dagger b_{q'}$ the amplitude is proportional to $\delta q$ which favours high momentum processes. Large momentum Umklapp processes invalidate the hydrodynamic description and moves the system into the diffusive regime. On a more fundamental level $U_{ph-ph} \sim \delta q$ corresponds to $\nabla x$ in real space, a manifestation of phonon's genuinely non local character – the acoustic phonons (which are those with linear dispersion) are in fact Goldstone bosons (pure phasons) corresponding to crystal lattice formation transition and it is conceptually difficult to imagine a density of an object that is generically defined in a non-local manner (as a relative motion in different cells). In our case, we study optical phonons where the density can be assigned to an amplitude of a local, intra-cell, vibration. Optical phonons are usually non-dispersive, but in $Bi_2Te_3$, resonant-band compound [25], a long-range vibron–vibron interactions have two effects: (i) lower the frequency $\omega_{TO}(q \rightarrow \Gamma)$ making the branch dispersive; (ii) change the

9

royalsocietypublishing.org/journal/rspa  Proc. R. Soc. A 476: 20200088

character of interaction by a factor $1/q$ making it $q$-independent (hence overall a purely local hard-core bosons model with $K_{ph} = 1$). It should be noted that the $K_{ph} = 1$ is also expected for weakly doped system of boson's band-insulator a regime that we expect to reach for large TO phonon density. Our description can be further improved by including interaction with the strain field. Recently, a concept of dislons has been introduced [19,20] that captures a quantized fluctuations of dislocation. It is expected that finite-$q$ phonons will entertain dislon mediated phonon-phonon $\sim q^2$, a further contribution to the long range lattice anharmonicity.

On general grounds we expect the following effects for the phonon dynamics [19]: for the uniform excitations ($q \approx 0$) since the strength of atomic forces close to dislocation is reduced the frequency $\omega_0$ will go down to zero (in bulk $Bi_2Te_3$ the energy of the lowest optical phonon [33] $\leq 1\,THz$). On the other hand we know that at high q there are phonon modes that due to confinement have frequencies higher than in the bulk. Finally, at intermediate frequencies the dislons [20] can mix various TO phonon branches leading to a continuous spectrum (and such closing of spectral gaps has been indeed observed). Finally, the resonant band effects, that are ascribed [25] to a non-local electronic polarization, shall be enhanced by the presence of TLL with collective $\chi_{TLL}$. Hence an expectation is that a quasi-continuous TO branch with larger bandwidth [33] will emerge.

A second issue is whether phonons can form 1D system on a dislocation. Recent molecular dynamics studies [34,35] found that these phonons are susceptible to dislocation as they can scatter on the strain field [18,21], as intuitively expected, and the anharmonic effects are enhanced close to a dislocation [20]. This has three implications: firstly, the phonon frequencies in the vicinity of dislocation are modified [19] (and their eigenvectors may be different as well) which reduces a direct hybridization between inner and outer crystal oscillations [35]; secondly, along the dislocation direction we need to include phonon-phonon anharmonic interaction effects; thirdly, in the directions perpendicular to a dislocation (more precisely a network of dislocations) the translation invariance of a pure crystal lattice is strongly broken and Bloch plane waves are not any longer a good eigenstates basis for the phonon system. This assertion, that the TO phonons are effectively trapped in a perpendicular direction, is an experimentally confirmed fact [2,15], and has been phenomenologically ascribed to interference effects between the dislocations [36] in agreement with our modelling, see equation (4.1) in the main text. As a result, their group velocity perpendicular to dislocation is much reduced [34]. We can then take the 1D formulae for the phonon correlation functions (hence original paper [28], not the erratum [37]).

The Fourier transforms are computed separately for electronic and phononic contributions. For each we perform the change of variables, which splits the integrals into functions of two independent variables $\xi_\pm = (x \pm V_{F,ph}t)/T$. These describe the 'light-cone' evolution of the system. The integrals themselves can be now completed using the following identities:

$$\int dz \mathrm{Exp}(izq)\mathrm{Sinh}^{-K}(z) = -\exp(z(iq+K))_2F_1(K, (K+iq)/2, 1+(K+iq)/2, \exp(z))/(K+iq)$$

$$\int dz \mathrm{Exp}(izq)\mathrm{Cosh}(z)\mathrm{Sinh}^{-K}(z)$$

$$= (-\exp(z(iq+K))_2F_1(1+K, (K+iq)/2, 1+(K+iq)/2, \exp(z))/(K+iq))$$

$$+ (-\exp(z(iq+K))_2F_1(1+K, (2+K+iq)/2, 1+(2+K+iq)/2, \exp(z))/(2+K+iq))$$

$$\int dz \mathrm{Exp}(izq)\mathrm{Coth}^2(z)\mathrm{Sinh}^{-K}(z) = \frac{\left(e^{-2x}-1\right)^{-K}\left(-e^{-4x}\left(e^{2x}-1\right)^2\right)^{K+1}\sinh^{-K-2}(x)}{\left(e^{2x}+1\right)^2}$$

$$\mathrm{AppellF1}[1/2(K-iq), -2, 2+K, 1/2(2+K-iq), -\exp(-2x), \exp(-2x)](K+iq) \tag{A 5}$$

where an identity $-\exp(z(iq+K))_2F_1(b,a,1+a,\exp(z))/a|_{z=0}^{z=\infty} = B(a, 1-b)$ can be used to simplify the results into a standard form of *Beta* functions. To generalize the hyperbolic function transforms

to account for a finite limits we use the following integral formula:

$$\int_{Z_1}^{Z_2} \mathrm{d}z z^a (1-z)^b = B_{\{z_1, z_2\}}(a+1, b+1), \tag{A 6}$$

where in our case $a = i\beta(\omega \pm V_i q) + K/2$, $b = 1 - K$, $z = \exp\left(-\frac{2\pi T \xi_\pm}{V_i}\right)$ with $V_i$ the velocity of either electronic of phononic particles. In a standard setting $z_1 = 0$, $z_2 = 1$ (which in the original $\xi$ language translates into $\xi_1 = \infty$, $\xi_2 = 0$ limits) and the above integral reduces to a standard Beta function. We see that by introducing the generalized incomplete Beta function we are able to selectively pick the zones of interest within the light cones distance domain. For instance, as described above the TO phonons fulfil the conditions of hydrodynamic regime only for the intermediate $q$-values, while the long-range (small $q$) part of a wave-packet may loose its quantum coherence (turn into diffusive region) due to interactions with dislons [20]. Then we need to exclude correlation between backscattering events that took place at distant light-cones. To capture it, we introduce a finite IR cut-off in $\xi_{ph}$ integral. We take $\xi_{tr}^{IR} = v_{ph}(\omega_0)^{-1}$ For the electronic liquid, the situation is opposite, while close to the $E_F$ the TLL is well defined, away from it the electrons can recombine with 3D carriers upon phonon absorption, the process becoming more intense with increasing $\omega$. So the back-scattering events for electrons cannot take place with to high frequency, the light-cones that are close to each other should be taken in bundles. To capture this effect we introduce a cut-off for smallest available $\xi$ in the integral that gives the $F_{el}$ correlations. Note, that this is despite the fact that there is a much larger UV cut-off for the existence of the TLL itself (of order of a fraction of eV), here we introduce an extra cut-off that characterizes transport properties $\xi_{tr}^{UV} = V_F(\Delta_d)^{-1}$, where $\Delta_d$ is a difference between CBM (where we put the chemical potential) and the convergence point of the $\Gamma$ point band with the TLL dispersion (so the difference between orange minimum and the point where green and dashed line converge in figure 2). Following [23], we take $\Delta_d \approx 0.15$ eV.

# References

1. Hicks LD, Dresselhaus MS. 1993 Thermoelectric figure of merit of a one-dimensional conductor. *Phys. Rev. B* **47**, 16 631–16 634. (doi:10.1103/PhysRevB.47.16631)
2. Poudel B *et al.* 2008 High-thermoelectric performance of nanostructured bismuth antimony telluride bulk alloys. *Science* **320**, 634–638. (doi:10.1126/science.1156446)
3. Chen YL *et al.* 2009 Experimental realization of a three-dimensional topological insulator, $Bi_2Te_3$. *Science* **325**, 178–181. (doi:10.1126/science.1173034)
4. Witting IT, Chasapis TC, Ricci F, Peters M, Heinz NA, Hautier G, Snyder GJ. 2019 The thermoelectric properties of bismuth telluride. *Adv. Electronic Mater.* **5**, 1800904. (doi:10.1002/aelm.201800904)
5. Ran Y, Zhang Y, Vishwanath A. 2009 One-dimensional topologically protected modes in topological insulators with lattice dislocations. *Nat. Phys.* **5**, 298–303. (doi:10.1038/nphys1220)
6. Murakami S, Takahashi R, Tretiakov OA, Abanov Ar., Sinova J. 2011 Thermoelectric transport of perfectly conducting channels in two- and three-dimensional topological insulators. *J. Phys: Conf. Ser.* **334**, 012013. (doi:10.1088/1742-6596/334/1/012013)
7. Krive IV, Romanovsky IA, Bogachek EN, Scherbakov AG, Landman U. 2001 Thermoelectric effects in a Luttinger liquid. *Low Temperature Phys.* **27**, 821–830. (doi:10.1063/1.1414571)
8. Szasz A, Ilan R, Moore JE. 2017 Electrical and thermal transport in the quasiatomic limit of coupled Luttinger liquids. *Phys. Rev. B* **95**, 085122. (doi:10.1103/PhysRevB.95.085122)
9. Ivanov YV. 2010 Ballistic thermoelectric transport in a Luttinger liquid. *J. Phys.: Condens. Matter* **22**, 245602. (doi:10.1088/0953-8984/22/24/245602)
10. Ström A, Johannesson H, Japaridze GI. 2010 Edge dynamics in a quantum spin hall state: effects from rashba spin-orbit interaction. *Phys. Rev. Lett.* **104**, 256804. (doi:10.1103/PhysRevLett.104.256804)
11. Hu L *et al.* 2018 Ubiquitous spin-orbit coupling in a screw dislocation with high spin coherency. *Phys. Rev. Lett.* **121**, 066401. (doi:10.1103/PhysRevLett.121.066401)
12. Schmidt TL, Rachel S, von Oppen F, Glazman LI. 2012 Inelastic electron backscattering in a generic helical edge channel. *Phys. Rev. Lett.* **108**, 156402. (doi:10.1103/PhysRevLett.108.156402)

13. Budich JC, Dolcini F, Recher P, Trauzettel B. 2012 Phonon-induced backscattering in helical edge states. *Phys. Rev. Lett.* **108**, 086602. (doi:10.1103/PhysRevLett.108.086602)

14. Kharitonov M, Geissler F, Trauzettel B. 2017 Backscattering in a helical liquid induced by rashba spin-orbit coupling and electron interactions: locality, symmetry, and cutoff aspects. *Phys. Rev. B* **96**, 155134. (doi:10.1103/PhysRevB.96.155134)

15. Kim SI *et al.* 2015 Dense dislocation arrays embedded in grain boundaries for high-performance bulk thermoelectrics. *Science* **348**, 109–114. (doi:10.1126/science.aaa4166)

16. Li G, Aydemir U, Morozov SI, Wood M, An Q, Zhai P, Zhang Q, Goddard WA, Snyder GJ. 2017 Superstrengthening $Bi_2Te_3$ through nanotwinning. *Phys. Rev. Lett.* **119**, 085501. (doi:10.1103/PhysRevLett.119.085501)

17. Deng R *et al.* 2018 Thermal conductivity in $Bi_{0.5}Sb_{1.5}Te_{3+x}$ and the role of dense dislocation arrays at grain boundaries. *Sci. Adv.* **4**, eaar5606. (doi:10.1126/sciadv.aar5606)

18. Liu Y, Li YY, Rajput D, Gilks S, Lari L, Galindo PL, Weinert M, Lazarov VK, Li L. 2014 Tuning dirac states by strain in the topological insulator $Bi_2Se_3$. *Nat. Phys.* **10**, 294–299. (doi:10.1038/nphys2898)

19. Li M, Cui W, Dresselhaus MS, Chen G. 2017 Electron energy can oscillate near a crystal dislocation. *New J. Phys.* **19**, 013033. (doi:10.1088/1367-2630/aa5710)

20. Li M, Tsurimaki Y, Meng Q, Andrejevic N, Zhu Y, Mahan GD, Chen G. 2018 Theory of electron–phonon–dislon interacting system–toward a quantized theory of dislocations. *New J. Phys.* **20**, 023010. (doi:10.1088/1367-2630/aaa383)

21. Kim H-S, Kang S, Tang Y, Hanus R, Snyder G. 2016 Dislocation strain as the mechanism of phonon scattering at grain boundaries. *Mater. Horiz.* **3**, 234–240. (doi:10.1039/C5MH00299K)

22. Yu. Yavorsky B, Hinsche NF, Mertig I, Zahn P. 2011 Electronic structure and transport anisotropy of $Bi_2Te_3$ and $Sb_2Te_3$. *Phys. Rev. B* **84**, 165208. (doi:10.1103/PhysRevB.84.165208)

23. Michiardi M *et al.* 2014 Bulk band structure of $Bi_2Te_3$. *Phys. Rev. B* **90**, 075105. (doi:10.1103/PhysRevB.90.075105)

24. Zhang JL *et al.* 2011 Pressure-induced superconductivity in topological parent compound $Bi_2Te_3$. *Proc. Natl Acad. Sci. USA* **108**, 24–28. (doi:10.1073/pnas.1014085108)

25. Lee S, Esfarjani K, Luo T, Zhou J, Tian Z, Chen G. 2014 Resonant bonding leads to low lattice thermal conductivity. *Nat. Commun.* **5**, 3525. (doi:10.1038/ncomms4525)

26. Citro R, Orignac E, Giamarchi T. 2005 Adiabatic-antiadiabatic crossover in a spin-Peierls chain. *Phys. Rev. B* **72**, 024434. (doi:10.1103/PhysRevB.72.024434)

27. Götze W, Wölfle P. 1972 Homogeneous dynamical conductivity of simple metals. *Phys. Rev. B* **6**, 1226–1238. (doi:10.1103/PhysRevB.6.1226)

28. Shimshoni E, Andrei N, Rosch A. 2003 Thermal conductivity of spin-$\frac{1}{2}$ chains. *Phys. Rev. B* **68**, 104401. (doi:10.1103/PhysRevB.68.104401)

29. Hamasaki H, Tokumoto Y, Edagawa K. 2017 Dislocation conduction in Bi-Sb topological insulators. *Appl. Phys. Lett.* **110**, 092105. (doi:10.1063/1.4977839)

30. Chudzinski P. 2019 Why it is so hard to detect luttinger liquids in angle resolved photo-emission spectroscopy? *J. Phys.: Condens. Matter* **31**, 105601. (doi:10.1088/1361-648X/aafa60)

31. Hufford ME, Davis HT. 1929 The diffraction of light by a circular opening and the Lommel wave theory. *Phys. Rev.* **33**, 589–597. (doi:10.1103/PhysRev.33.589)

32. Monserrat B, Vanderbilt D. 2016 Temperature effects in the band structure of topological insulators. *Phys. Rev. Lett.* **117**, 226801. (doi:10.1103/PhysRevLett.117.226801)

33. Jenkins JO, Rayne JA, Ure RW. 1972 Elastic moduli and phonon properties of $Bi_2 Te_3$. *Phys. Rev. B* **5**, 3171–3184. (doi:10.1103/PhysRevB.5.3171)

34. Sun Y, Zhou Y, Jian H, Liu W, Nan C, Lin Y, Hu M, Xu B. 2019 Strong phonon localization in PbTe with dislocations and large deviation to Matthiessen's rule. *npj Comput. Mater.* **5**, no. 97. (doi:10.1038/s41524-019-0232-x)

35. Song H, Zhang H, Xiong S, Zhang H, Wang H, Chen Y, Volz S, Ni Y. 2019 Screw dislocation induced phonon transport suppression in SiGe superlattices. *Phys. Rev. B* **100**, 075432. (doi:10.1103/PhysRevB.100.075432)

36. Li F-F, Wang H-X, Xiong Z, Lou Q, Chen P, Wu R-X, Poo Y, Jiang J-H, John S. 2018 Topological light-trapping on a dislocation. *Nat. Commun.* **9**, 2462. (doi:10.1038/s41467-018-04861-x)

37. Shimshoni E, Andrei N, Rosch A. 2005 Erratum: thermal conductivity of spin-$\frac{1}{2}$ chains [*Phys. Rev. B* **68**, 104401 (2003)]. *Phys. Rev. B* **72**, 059903. (doi:10.1103/PhysRevB.72.059903)